Scientific Report

SOURCE DATA | TRANSPARENT PROCESS

EMBO reports

# A single MIU motif of MINDY-1 recognizes K48-linked polyubiquitin chains

Yosua Adi Kristariyanto, Syed Arif Abdul Rehman, Simone Weidlich, Axel Knebel & Yogesh Kulathu*

## Abstract

**The eight different types of ubiquitin (Ub) chains that can be formed play important roles in diverse cellular processes. Linkage-selective recognition of Ub chains by Ub-binding domain (UBD)-containing proteins is central to coupling different Ub signals to specific cellular responses. The motif interacting with ubiquitin (MIU) is a small UBD that has been characterized for its binding to monoUb. The recently discovered deubiquitinase MINDY-1/FAM63A contains a tandem MIU repeat (tMIU) that is highly selective at binding to K48-linked polyUb. We here identify that this linkage-selective binding is mediated by a single MIU motif (MIU2) in MINDY-1. The crystal structure of MIU2 in complex with K48-linked polyubiquitin chains reveals that MIU2 on its own binds to all three Ub moieties in an open conformation that can only be accommodated by K48-linked triUb. The weak Ub binder MIU1 increases overall affinity of the tMIU for polyUb chains without affecting its linkage selectivity. Our analyses reveal new concepts for linkage selectivity and polyUb recognition by UBDs.**

**Keywords** MINDY deubiquitinase; motif interacting with ubiquitin; polyubiquitin; ubiquitin binding domain; ubiquitin signaling
**Subject Categories** Post-translational Modifications, Proteolysis & Proteomics; Signal Transduction; Structural Biology
**DOI** 10.15252/embr.201643205 | Received 12 August 2016 | Revised 13 December 2016 | Accepted 16 December 2016 | Published online 12 January 2017
**EMBO Reports (2017) 18: 392–402**

## Introduction

Ubiquitylation is a protein modification that regulates a plethora of cellular signaling [1–4]. The 76-residue ubiquitin (Ub) is attached to Lys residues of target substrates through an enzymatic cascade that involves Ub-activating enzyme (E1), Ub-conjugating enzyme (E2), and Ub-ligating enzyme (E3) [5]. Ub itself has seven Lys residues and an N-terminal Met residue that can be ubiquitylated, which results in the formation of eight types of polyubiquitin (polyUb) chains: M1, K6, K11, K27, K29, K33, K48, and K63 [6]. The different chain types are associated with different cellular functions, and they adopt distinct conformations. For example, K48-linked polyUb chains that target proteins for proteasomal degradation adopt compact conformations [7]. Indeed, K48-linked polyUb chains have also been observed in open conformations, reflecting the flexible nature of polyUb chains [8,9]. Proteins containing Ub-binding domains (UBDs) recognize these distinct conformations of polyUb chains and translate the different Ub signals to produce distinct outcomes [10]. Since Ub signals regulate diverse cellular processes, they have to be removed and regulated, and this function is mainly performed by dedicated proteases called deubiquitinating enzymes (DUBs) [11].

To date, there are 21 families of UBDs reported, which vary in size, structure, and mode of binding with Ub [10,12]. Ub-interacting motif (UIM) and motif interacting with Ub (MIU) are the smallest among the UBDs. Both motifs form an α-helical structure composed of ~20 residues [13–16]. They bind to monoUb through hydrophobic residues centered on a key alanine that interacts with the hydrophobic I44 patch (L8, I44, H68, and V70) on Ub. The signature motif of the MIU is the inverse of a UIM, which explains why monoUb binds MIU in a reverse orientation than when bound to UIM [15,16].

The affinity of a UIM for monoUb is relatively weak with dissociation constants ($K_d$) in the range of 100 μM to 2 mM [17]. The MIU of Rabex-5 has slightly higher affinity for monoUb at ~30 μM [15,16]. To compensate for the weak affinities, many proteins contain arrays of more than one UIM or MIU motifs, which provide avidity to bind polyUb chains with relatively higher affinity [13,15,16,18–21]. In some UBDs, these arrangements also determine the linkage-selective binding for polyUb. For instance, in the tandem UIM of Rap80, each UIM motif binds to a single Ub and the linker between the two motifs determines the orientation of the binding surfaces on the individual UIMs, thereby imparting specificity in binding to polyUb of K63 linkage type [18,19].

We recently reported the discovery of a new family of DUBs called MINDY (MIU-containing novel DUB family) that is highly selective at cleaving K48-linked polyUb chains [22]. The first member identified in this family, FAM63A/MINDY-1, contains a tandem MIU repeat (tMIU) that is highly specific for binding to K48-linked polyUb chains. The tMIU enables efficient cleavage of long polyUb chains by MINDY-1. In order to understand the molecular mechanism of how the tMIU of MINDY-1 specifically recognizes K48 chains, we biochemically and biophysically analyzed its Ub binding in detail. Our results reveal an atypical mode of polyUb recognition where the second MIU (MIU2) on its own contains all the specificity determinants. MIU2 makes contacts with all three Ub

MRC Protein Phosphorylation and Ubiquitylation Unit, School of Life Sciences, University of Dundee, Dundee, UK
*Corresponding author. Tel: +44 1382 388163; Fax: +44 1382 223778; E-mail: ykulathu@dundee.ac.uk

moieties in a K48-linked polyUb chain via three different binding sites on the MIU. The first MIU (MIU1) further contributes to polyUb binding through avidity despite itself being a poor binder for polyUb chains. Collectively, our results provide new concepts for polyUb recognition by MIU motifs.

## Results and Discussion

### MINDY-1 contains a tandem MIU repeat, highly selective at binding K48-polyUb chains

Preferences of tandem UIMs for binding to one linkage type of polyUb chains over the other have been described [13,18,19,23]. However, such analyses were limited to only few chain types, mostly K48 and K63 linkages. Only recently, enzymatic methods to assemble large quantities of pure polyUb chains of M1, K6, K11, K29, K33, K48, and K63 were established [24–31]. These chains are invaluable reagents for UBD linkage profiling that led for instance to the identification of NZF1 of TRABID as a K29- and K33-polyUb selective binder [27]. When profiled against tetraUb of seven linkage types, we confirmed the exclusive preference of Rap80 and Epsin-15 tUIMs for binding to K63 polyUb chains [18,19] (Fig EV1A). We found that S5a tUIM that was previously reported to bind K11, K48, and K63 chains also captures M1 polyUb chains [23,32] (Fig EV1A). The tandem A20_ZnF-MIU domain of Rabex-5 previously reported to capture M1-, K48-, and K63-polyUb chains [15,16,33,34] also binds to tetraUb linked via K6, K11, K29, and K33 (Fig EV1A). Our results demonstrate that using a panel of tetraUb chains in Halo-tagged UBD pull-down assays can reveal the linkage preference of a given UBD.

Based on sequence analysis, we discovered that two previously uncharacterized proteins, FAM63A and FAM63B, contain a tandem repeat of two MIU motifs at the C-terminus (Figs 1A and B, and EV1B and C). In our recent study, we characterized these two proteins to be DUBs of a novel family, which we named MINDY (MIU-containing novel DUB family) [22]. While the sequences of the MIU motifs are highly conserved between the two proteins, the linker region connecting the two motifs is not (Fig 1A). Despite this similarity, the tMIU of FAM63A/MINDY-1 is highly specific for binding to K48 chains, whereas the tMIU of FAM63B/MINDY-2 is non-specific and binds to polyUb chains of different linkage types (Fig 1C). We therefore wanted to understand how the tMIU of MINDY-1 achieves linkage specificity for K48 chains.

### Single MIU motif is sufficient for selective binding to K48 chains

We first evaluated the contribution of each MIU motif of MINDY-1 towards polyUb binding. Mutating the key central alanine of the MIU motif to glycine has been reported to disrupt the motif from binding to monoUb [16]. We therefore mutated the central alanine or deleted the whole motif of MIU1 or MIU2 and tested the effect of such mutations on K48-linked tetraUb binding. Mutating or deleting MIU1 did not disrupt binding to K48-tetraUb (Fig 2A, lanes 4 and 6). In contrast, mutating or deleting MIU2 completely abolished binding to K48-tetraUb (Fig 2A, lanes 3 and 5). These observations were further confirmed in pull-down assays of ubiquitylated materials from HEK293 cells (Fig 2B). Together, our data suggest that MIU2 is the dominant polyUb chain binder in MINDY-1.

Tandem UIMs and MIUs have been reported to prefer binding to longer polyUb chains [13,16,20,21,35–38]. Pull-downs from HEK293 cell extracts using MINDY-1 tMIU did not capture lower molecular weight polyUb chains, suggesting a preference for binding to longer polyUb chains (Fig 2B). To investigate this further, we incubated Halo-tagged tMIU with K48-linked polyUb chains of different lengths that varied from monoUb to pentaUb (Fig 2C). We found that the tMIU binds to tri-, tetra-, and pentaUb, but does not bind to monoUb and diUb, supporting a preference of tMIU to bind longer polyUb chains. To measure the affinity of the tMIU for polyUb chains of varying lengths, we performed ITC measurements where MINDY-1 tMIU was titrated into either K48-diUb, triUb, or tetraUb (Fig 2D–F). We observed affinities of 23 μM, 1.2 μM, and 185 nM for diUb, triUb, and tetraUb, respectively, suggesting that the affinity of MINDY-1 tMIU for polyUb chains increases with chain length. Collectively, our results demonstrate that MINDY-1 tMIU preferably binds to longer K48-linked polyUb chains.

To explore the role of MIU1 in the binding of MINDY-1 tMIU to polyUb chains, we compared the binding of MIU1 and MIU2 on their own to K48-triUb by ITC. If MIU1 has no role in overall binding, we predict the affinity of MIU2 for K48-triUb to be the same as that observed with tMIU. Consistent with our previous finding, MIU1 on its own has no measurable affinity toward polyUb chains (Fig 2G). Surprisingly, we found that the affinity of the tMIU containing both MIU1 and MIU2 for K48-triUb is 10-fold higher than that of MIU2 on its own (Fig 2H). This suggests that even though the affinity of the isolated MIU1 for K48-triUb is negligible, it contributes to tMIU binding through avidity.

Since MIU1 only provides weak binding to polyUb chains, we hypothesize that MIU2 is the main determinant of K48-linkage selectivity. When Halo-tagged MIU2 was incubated with a panel of seven types of polyUb chains, it only captured K48-tetraUb (Fig 2I). This implies that on its own MIU2 is still selective for K48 linkages and is therefore the linkage specificity determinant in MINDY-1 tMIU.

### Cooperativity between MIU1 and MIU2 results in highly selective polyUb interaction

Even though MIU2 is sufficient to capture K48-linked polyUb chains, MIU1 is still required for the tMIU to bind polyUb chains with higher affinity. However, it remains unclear whether MIU1 also contributes to the overall linkage selectivity of the tMIU. To address this, we first explored the contribution of the linker separating the two motifs. One major difference between the K48-linkage-specific MINDY-1 tMIU and the linkage-unspecific MINDY-2 tMIU is their linker length and composition (Fig 1A). In Rap80, the linker length in between two UIM motifs defines the specificity for K63-linked polyUb [18,19]. Therefore, to test whether the linker length and composition of MINDY-1 tMIU regulate polyUb binding, we replaced the 5-residue linker of MINDY-1 tMIU with the one of MINDY-2 tMIU. Swapping the linker made no difference to linkage specificity of the tMIU (Fig 3A, lane 6). The presence of two proline residues results in a rigid linker (Fig 1A). To make the linker relatively flexible, we mutated the two proline residues to alanine or replaced the whole linker with poly-Ser-Gly or poly-Ala linker (Fig 3A, lanes 7–9). Again, we found that altering the composition of the linker does not convert the K48-linkage specificity of the tMIU. In

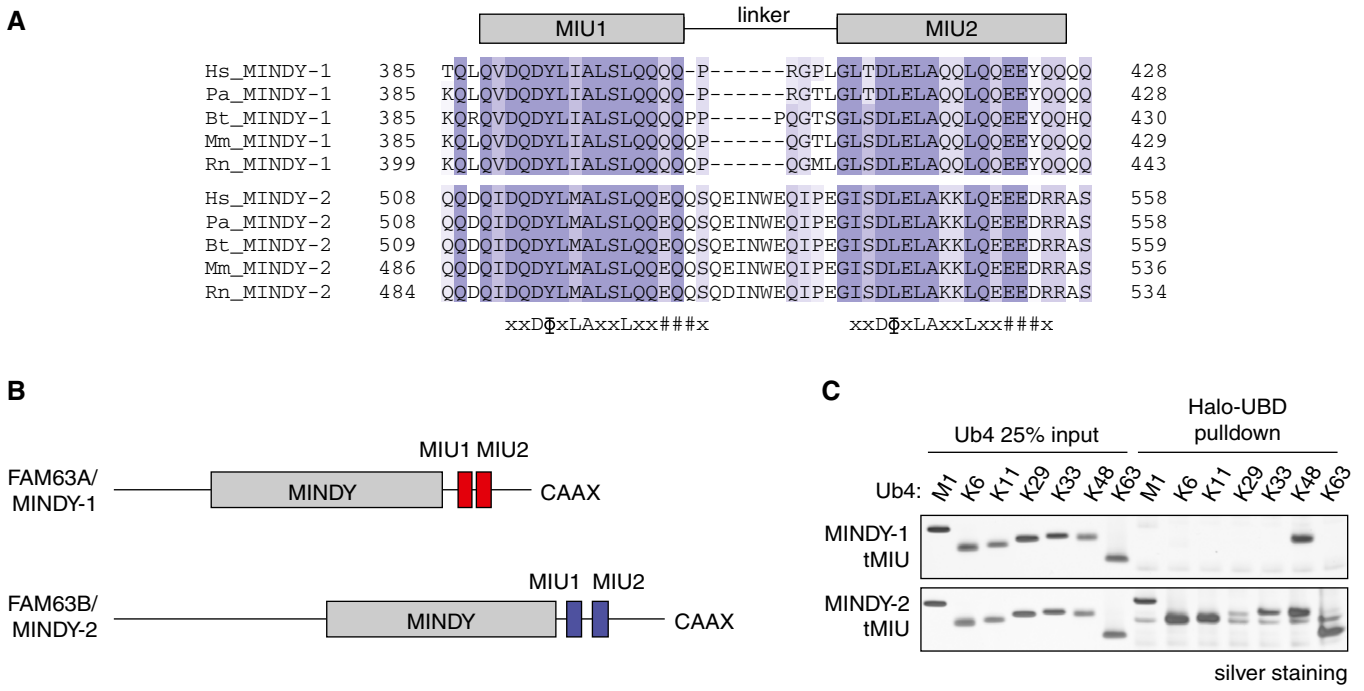


**Figure 1. Linkage selectivity in tandem MIU repeats of MINDY-1.**

A Sequence alignment of MINDY-1/FAM63A and MINDY-2/FAM63B tMIUs from different species. MIU1, MIU2, and the tMIU linker are indicated. The conserved motif of MIU is shown: ϕ, large hydrophobic; #, acidic; x, any residues. Hs, *Homo sapiens*; Pa, *Pongo abelii*; Bt, *Bos taurus*; Mm, *Mus musculus*; Rn, *Rattus norvegicus*. Protein sequences were retrieved from UniProt database, aligned using the ClustalO program, and edited with the Jalview software [59].

B Schematic representation of MINDY-1 and MINDY-2 domains. The MIU motifs of MINDY-1 and MINDY-2 are colored red and blue, respectively.

C PolyUb linkage selectivity profiling for MINDY-1 and MINDY-2 tMIU. TetraUb chains of the indicated linkage types (29 pmol) were incubated with 1.05 nmol Halo-tagged tMIU of MINDY-1 or MINDY-2 immobilized on HaloLink resin for 2 h at 4°C. The captured materials were separated on 4–12% Bis-Tris gels and visualized by silver staining.

Source data are available online for this figure.

summary, the length and composition of the linker do not affect the specificity of MINDY-1 tMIU for K48-linked polyUb chains.

Despite being very similar to the tMIU of MINDY-1, it is intriguing that the tMIU of MINDY-2 binds to polyUb chains of all linkage types (Fig 1C). We therefore characterized the binding properties of the individual MIU motifs of MINDY-2 and found that the first MIU (MIU1) motif of MINDY-2 is the dominant Ub binder, whereas the second motif (MIU2) shows no detectable binding (Fig 3B). Further, MINDY-2 MIU1 has no linkage selectivity as it captures polyUb chains of all linkage types (Fig 3C). The affinity of MINDY-2 MIU1 on its own to polyUb chains is weaker compared to the tMIU (Figs 3C and 1C). This suggests that similar to MINDY-1, the weak polyUb-binder MIU2 in MINDY-2 also contributes to overall polyUb binding of the tMIU through avidity.

We then wondered whether replacing MIU1 of MINDY-1 with a motif that binds non-selectively to polyUb chains could alter the linkage preference of MINDY-1 tMIU. First, we tested whether introducing a K48-selective MIU at the position of MIU1 alters the specificity of the tandem MIU. When analyzed, a tandem repeat of the K48-selective MINDY-1 MIU2 is still K48-linkage selective and in fact appears to bind to K48 chains with higher affinity (Fig 3D top). Next, we performed a domain swap, where we replaced MINDY-1 MIU1 with the non-selective polyUb binder of MINDY-2 MIU1. The hybrid tMIU is no longer K48-selective and binds to K6, K11, K48, and K63 chains, which is similar to the profile of MINDY-2 tMIU (Fig 3D bottom and Fig 1C). Thus, within the tMIU, having a non-selective polyUb binder at the position of MIU1 converts the K48-specific binder to a non-specific one. In summary, the weak polyUb-binding property of MIU1 allows MIU1 to work in synergy with MIU2 to increase the affinity of MINDY-1 tMIU for polyUb without altering its selectivity for K48-linked polyUb chains.

### MIU2 binds to open conformations of K48-linked polyUb chains

To understand how MINDY-1 MIU2 specifically recognizes K48-linked polyUb and how this interaction is enhanced by MIU1, we attempted to crystallize the tMIU in complex with K48-triUb. Unfortunately, we were unable to obtain any crystals. We therefore crystallized the tMIU in complex with K48-diUb and these crystals diffracted to 2.0 Å. The structure was solved by molecular replacement using Ub as a search model. There are two Ub moieties present in the asymmetric unit (ASU) (Fig 4A). Although discernible electron density is not present for the linkage between the two Ub moieties, L73 of the distal Ub is pointing towards K48 of the proximal Ub. Clear electron density was visible for a helix, which was manually built in and the structure was refined to the final statistics shown in Appendix Table S1. To our surprise, only one 4-turn-helix corresponding to MIU2 (residues 408–426) could be modeled into

 

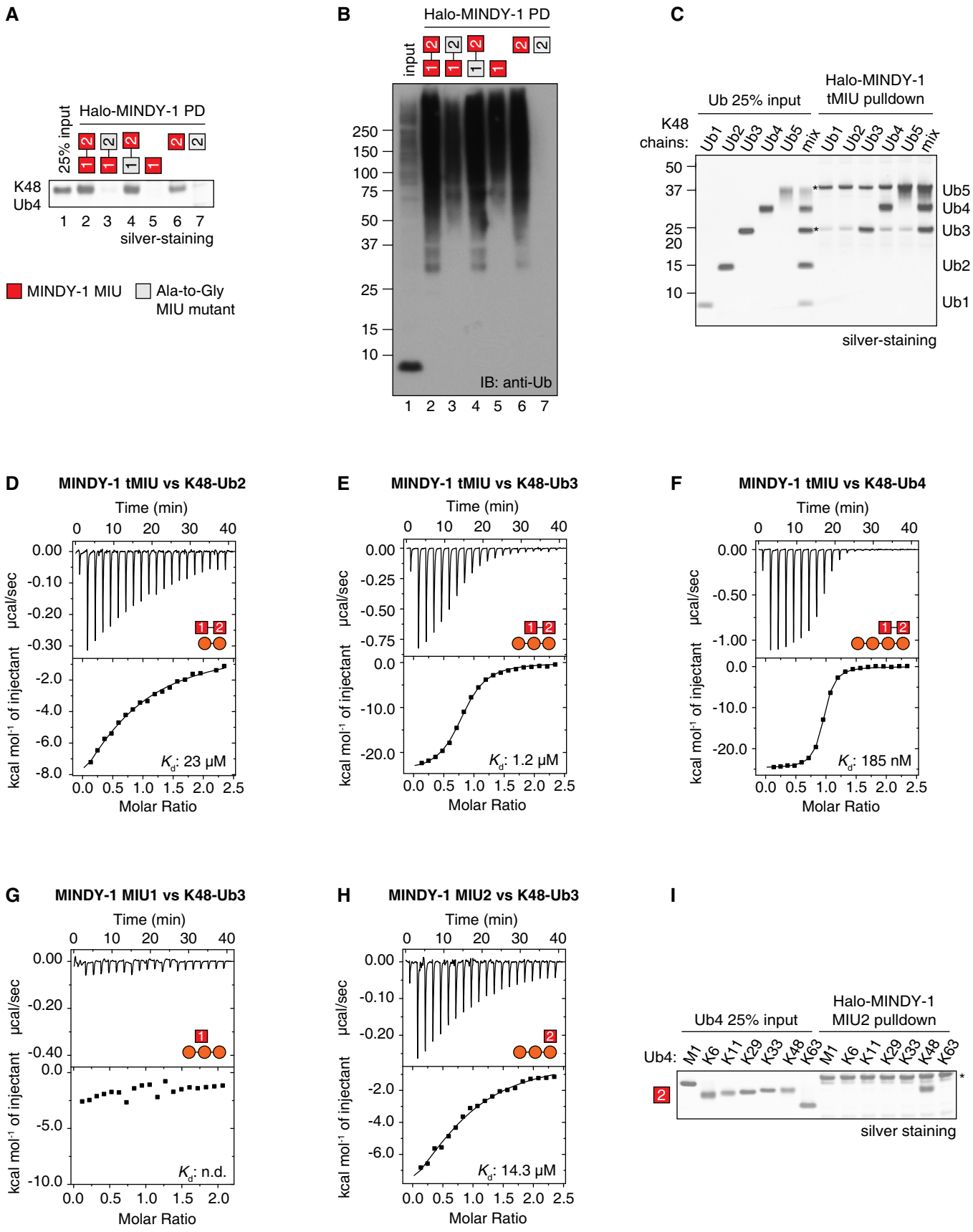


**Figure 2.**

**Figure 2. MINDY-1 MIU2 is sufficient for binding to K48 chains.**

A K48-linked tetraUb chains were captured by Halo-tagged tMIU wild type or mutants of MINDY-1 as in Fig 1C. Red and gray squares indicate wild-type and mutant MIU (Ala-to-Gly), respectively. PD, pull-down.

B HEK293 cell lysates (1 mg) were incubated with 1.05 nmol Halo-tagged tMIU wild type or mutants. The captured Ub was visualized by anti-Ub immunoblotting.

C MonoUb and K48-linked polyUb chains of different lengths (29 pmol each) were incubated with 1.05 nmol of Halo-tagged tMIU. The captured materials were visualized as in Fig 1C. Asterisks indicate non-specific bands from Halo-UBD, which exhibit a similar electrophoretic mobility as tri- and pentaUb.

D–F ITC measurements for MINDY-1 tMIU binding to K48-linked diUb (D), triUb (E), and tetraUb (F). $K_d$ value of each measurement is indicated.

G, H ITC measurements for MINDY-1 MIU1 (G) and MIU2 (H) binding to K48-linked triUb. $K_d$ value of each measurement is indicated.

I PolyUb linkage selectivity assay of MINDY-1 MIU2 was carried out as in Fig 1C. Asterisk indicates non-specific bands from Halo-UBD.

Source data are available online for this figure.

the electron density. The weak affinity of MIU1 for polyUb chains (Fig 2G) and the unstructured linker connecting the two MIU motifs might explain the absence of electron density for MIU1.

Interestingly, when we analyzed the crystal packing, we found that the diUb from the ASU makes contact with the diUb from the symmetry-related molecule, forming a cyclic K48-linked tetraUb chain (Fig 4B). This cyclic chain adopts a doughnut-like shape with two grooves at its center where the two MIU2 molecules bind (Fig EV2A). The hydrophobic I44 patches are no longer at the interface between Ub moieties, and therefore, this cyclic K48-tetraUb chain is in an open conformation.

To date, four structures of K48-tetraUb chains have been solved [8,39–41]. In three of these structures (1F9J, 2O6V, and 3ALB), K48-linked tetraUb forms cyclic chains. However, these are all in closed conformations where the I44 patches of all the Ub moieties are buried in the interface (Fig 4C middle). Even though the other crystal structure of K48-tetraUb is in an open conformation (1TBE), the fourth and the first Ub moieties are not linked and therefore is a non-cyclic chain and different from the K48-tetraUb chain observed in this study (Fig 4C right). Interestingly, looking further into the symmetry-related molecules, we can also model an open non-cyclic K48-tetraUb (Fig EV2B). However, the distance between K48 and G76 of the second and third Ub moieties (~11 Å) is too far apart for an isopeptide bond to form. Therefore, this conformation is less likely to exist in nature. In summary, we here report a novel structure of open cyclic K48-linked tetraUb chains when in complex with two MINDY-1 MIU2 motifs.

### Mechanism of K48-linked triUb recognition by MIU2

The four Ub moieties of the cyclic K48-tetraUb chain are wrapped around the two MIU2 helices (Fig 4B). In such an arrangement, a

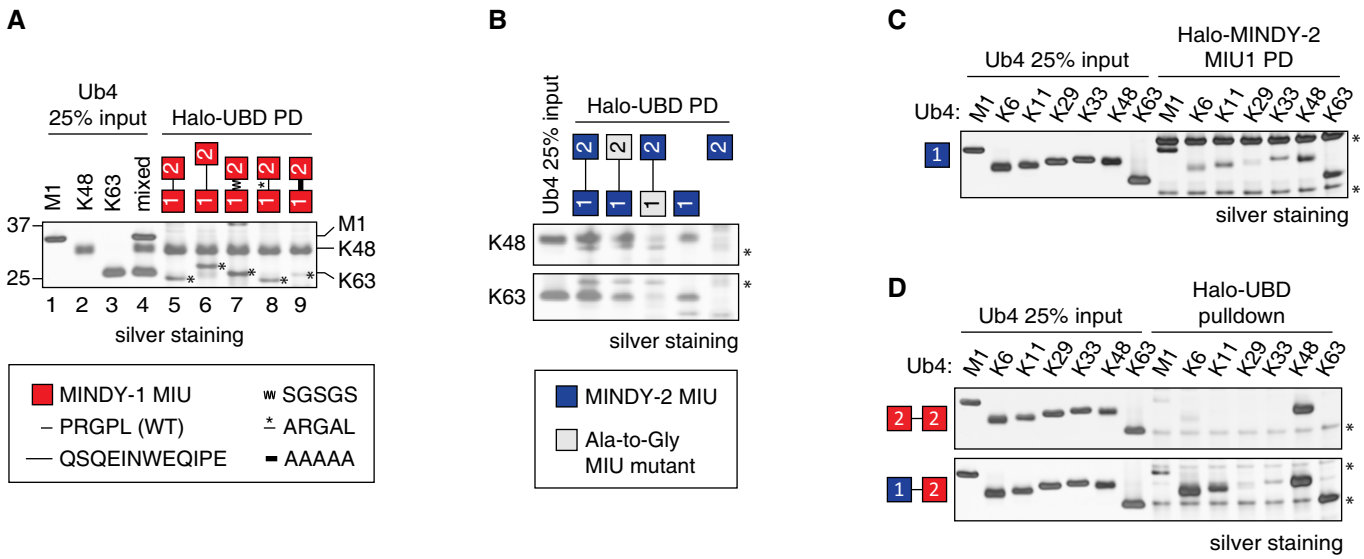


**Figure 3. Synergy between MIU1 and MIU2 in polyUb binding.**

A M1-, K48-, and K63-tetraUb chains were mixed in equal amount of 29 pmol each and incubated with 1.05 nM Halo-MINDY-1 tMIU with wild-type or mutant linkers. The captured materials were analyzed as in Fig 1C. Asterisks indicate non-specific bands from Halo-UBD, which run at a similar electrophoretic mobility as K63-tetraUb. PD, pull-down.

B K48- or K63-linked tetraUb chains were captured by Halo-tagged tMIU wild type or mutants of MINDY-2 as in Fig 2A. Blue and gray squares indicate wild-type and mutant MIU (Ala-to-Gly), respectively. Asterisks indicate non-specific bands from Halo-UBD.

C PolyUb linkage selectivity assay of MINDY-2 MIU1 was carried out as in Fig 1C. Asterisks indicate non-specific bands from Halo-UBD.

D PolyUb linkage selectivity assays of hybrid tMIUs were carried out as in Fig 1C. The first MIU motif of MINDY-1 tMIU was replaced by MINDY-1 MIU2 (top) or MINDY-2 MIU1 (bottom). Asterisks indicate non-specific bands from Halo-UBD, which have a similar electrophoretic mobility as M1- and K63-tetraUb chains.

Source data are available online for this figure.

 

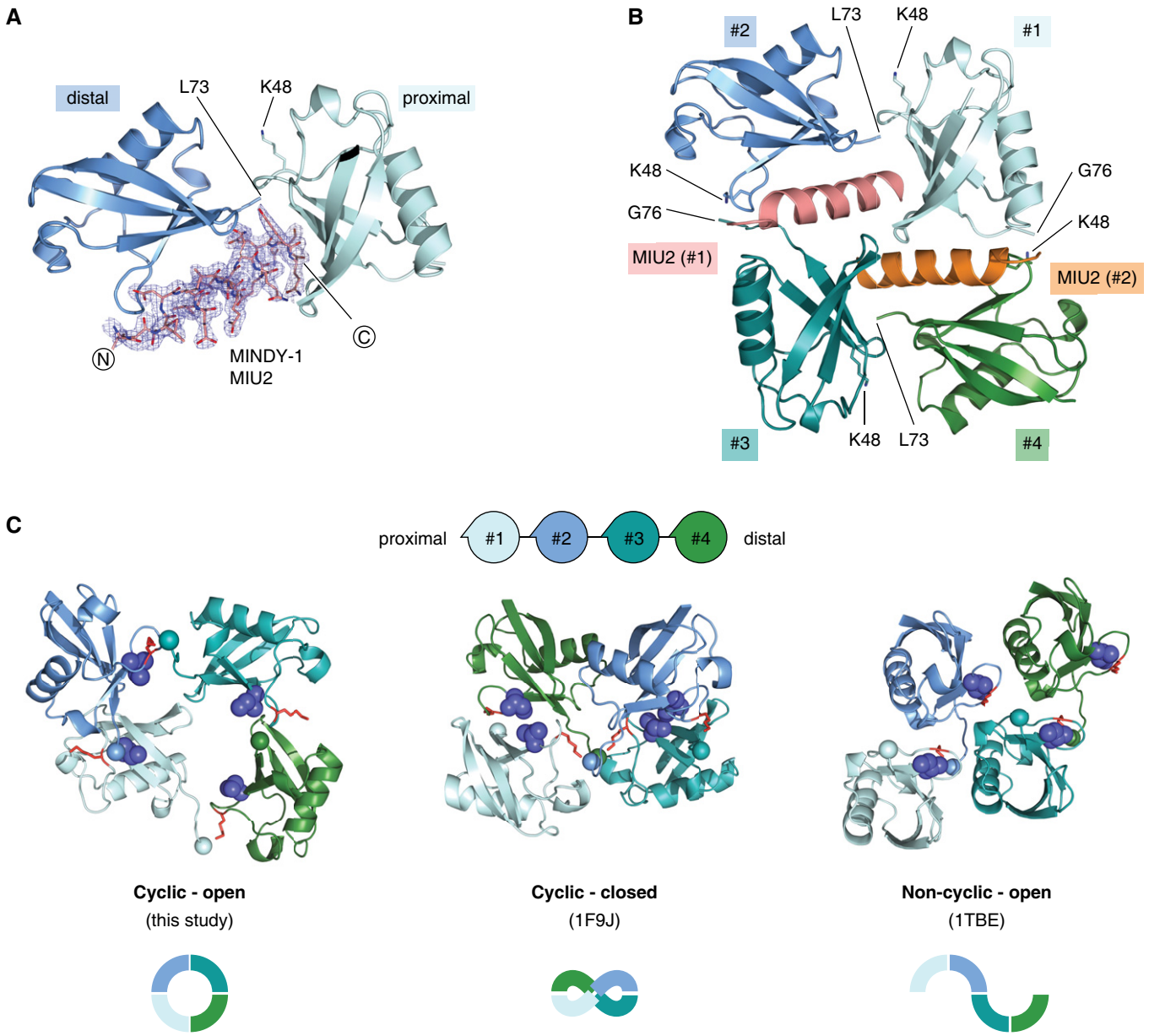


**Figure 4. Crystal structure of K48-diUb in complex with MINDY-1 MIU2.**

A Structure of MINDY-1 MIU2 and K48-diUb complex within an asymmetric unit (ASU) with $2|F_O|-|F_O|$ (blue) electron density maps for MIU2 contoured at 1σ. Proximal (light cyan) and distal (blue) are in cartoon representation and MIU2 (salmon) is in sticks.

B Open cyclic K48-linked tetraUb chains. Ub moiety #1 (light cyan), #2 (blue), and MIU2 moiety #1 (salmon) are from the ASU. Ub moiety #3 (teal), #4 (green), and MIU2 moiety #2 (orange) are from the symmetry-related molecules. K48 and the C-terminal tail of Ub moieties are indicated.

C Comparison of different K48-linked tetraUb conformations. Schematic diagram illustrates the coloring and numbering of Ub moieties, which are the same as for (B). K48 and C-terminal tail are shown in red sticks and spheres, respectively. For simplicity, only I44 is shown in blue spheres to represent the hydrophobic I44 patch (L8, I44, H68, and V70). PDB ID: 1TBE [8] and 1F9J [39].

single MIU2 interacts simultaneously with three Ub moieties using three different binding sites on the MIU2 helix (Figs 5A and B, and EV3A). Only K48-linked polyUb chains can adopt this conformation, as K48 is the only lysine residue within close proximity to the C-terminus of the distal Ub (Fig EV3B). This structure of MIU2 with K48-linked triUb explains the preference of MINDY-1 to bind to longer polyUb chains (Fig 2).

The first binding interface (Site 1) is formed through hydrophobic interactions and hydrogen bonds between MIU2 and the middle Ub (Figs 5C and EV3C). This mode of binding is similar to the one reported for Rabex-5 MIU and monoUb [15,16]. The conserved A416 of MIU2 is buried deep within the I44 patch of the middle Ub. As with other MIUs and UIMs, mutation of A416 completely abolishes polyUb binding (Figs 5F and EV4C). L413, L415, and L419 that

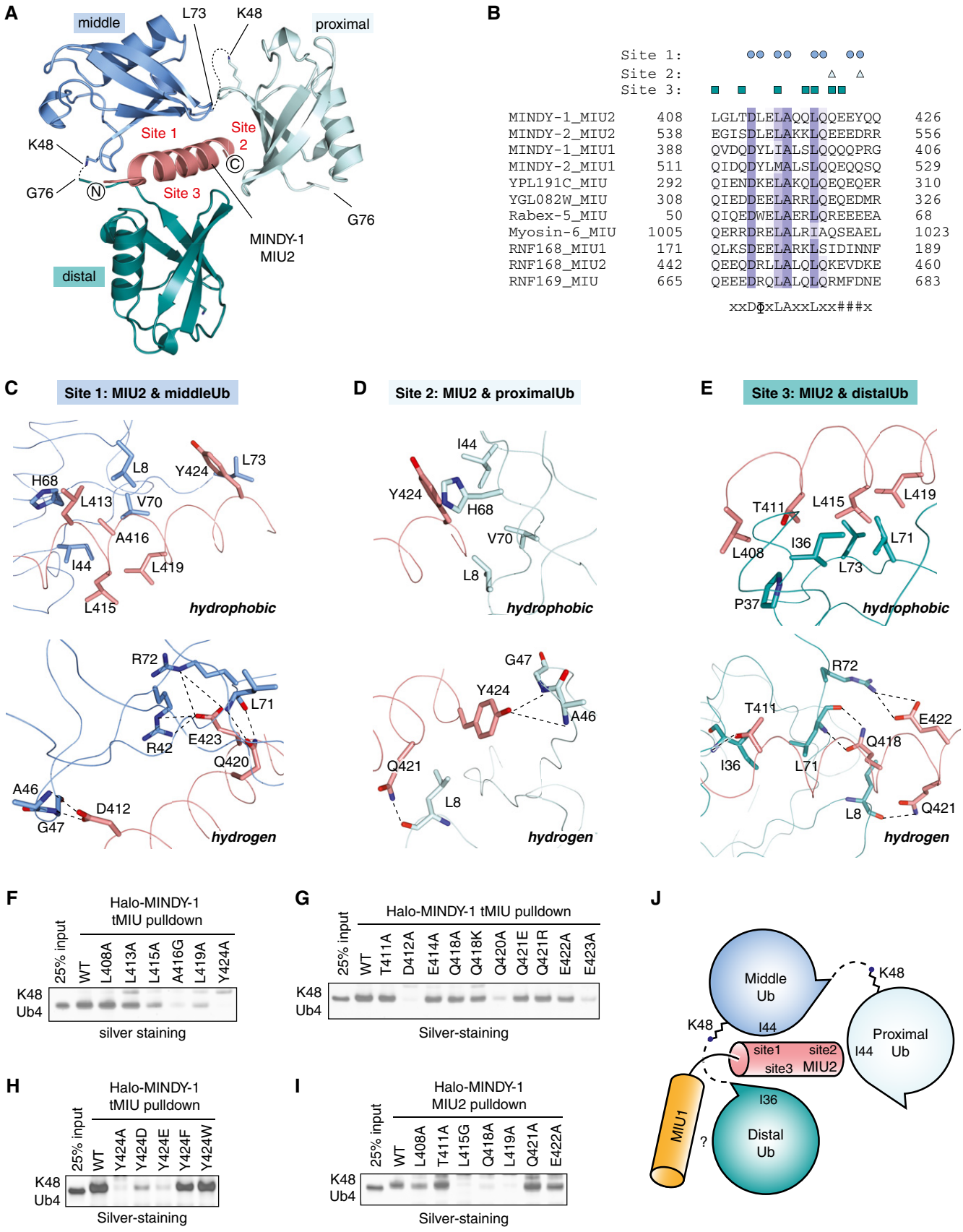


**Figure 5.**

**Figure 5. Mechanism of polyUb chain recognition by MIU2.**

A Structure of MIU2 in complex with K48-linked triUb is shown in cartoon. K48-triUb proximal (light cyan) and middle (blue) Ub are from the asymmetric unit, while the distal Ub (teal) is from a symmetry-related molecule (Fig 4B). K48 and the C-terminal tail of Ub, the three Ub binding sites on MINDY-1 MIU2 are indicated.

B Sequence alignment of MIU motifs from various proteins. All sequences are from *H. sapiens*, except for YPL191C and YGL082W, which are from *S. cerevisiae*. Residues of MINDY-1 MIU2 that form the three Ub-binding sites are indicated. The conserved motif of MIU is shown: ϕ, large hydrophobic; #, acidic; x, any residues.

C–E Close-up views of interactions between MINDY-1 MIU2 and the middle Ub (Site 1), proximal Ub (Site 2), or distal Ub (Site 3). Hydrophobic interactions and hydrogen bonds are shown on the top and bottom panels, respectively. Residues at the interface are shown in sticks and colored as in (A). Dotted lines indicate hydrogen bonds.

F, G Residues of MIU2 involved in hydrophobic interactions (F) and hydrogen bonds (G) were mutated, and the effect on tMIU binding to K48-tetraUb was investigated as in Fig 2A.

H Role of Y424 in tMIU binding to K48-tetraUb was investigated by mutating MIU2 Y424 to the indicated residues, and pull-down assays were performed as in Fig 2A.

I Residues of MIU2 forming Site 3 binding site were mutated, and the effect on MIU2 binding to K48-tetraUb was investigated as in Fig 2A.

J A model of how MINDY-1 tMIU achieves its K48-linkage selectivity. Three Ub-binding sites on MIU2 engage the I44 patches of the middle and proximal Ub, and the I36 patch of the distal Ub. MIU1 provides additional interactions with the distal Ub to increase overall binding affinity.

Source data are available online for this figure.

surround A416 also contribute in binding to I44 patch. The hydrogen bonds are formed between the side chains of D412 and Q420 and the main chains of Ub A46, G47, and L71. In addition to this, the side chains of MIU2 Q420 and Ub R42 and R72 also interact. Indeed, mutating residues D412, Q420, or E423 on MIU2 significantly reduces tMIU binding to K48-tetraUb, highlighting the importance of these Site 1 interactions (Fig 5G). Collectively, these networks of hydrophobic interactions and hydrogen bonds suggest a tight binding of the middle Ub to MIU2.

The second binding interface (Site 2) is formed between MIU2 and the proximal Ub, which occupies a smaller buried surface area of ~240 $Å^2$ in comparison with Site 1 (~500 $Å^2$) and Site 3 (~480 $Å^2$) (Fig 5A). The proximal Ub is bound by MIU2 in an unusual way, where a bulky hydrophobic residue on Site 2, Y424, mediates key interactions—the hydrophobic aromatic ring of Y424 interacts with the I44 patch of the proximal Ub, and the hydroxyl group of Y424 interacts with the main chain amide group of A46 and G47 (Fig 5D). These interactions are analogous to MIU2 A416 and D412 on Site 1, respectively (Fig 5C). Mutating Y424 to Ala or acidic residues, but not Phe or Trp, abolishes tMIU binding to K48-tetraUb, confirming the crucial role of the hydrophobic aromatic ring for Ub binding (Fig 5H). Y424 also interacts with L73 of the middle Ub and therefore highlights the key role of Y424 in stabilizing MIU2 interaction with polyUb. In other MIU motifs, the position corresponding to Y424 is commonly occupied by acidic residues, and therefore, the mode of binding by Y424 is a unique feature of MINDY-1 MIU2 (Fig 5B).

The third binding interface (Site 3) is formed between MIU2 and the distal Ub, which was determined from crystal contacts with the symmetry-related molecule (Fig 4A and B). MIU2 L408, T411, L415, and L419 interact with the hydrophobic patch on the distal Ub formed by I36, P37, L71, and L73 (Fig 5E). In addition, the side chains of MIU2 T411, Q418, and Q421 form hydrogen bonds with the main chains of Ub I36, L71, and L8, respectively. Further interactions between the side chains of MIU2 E422 and Ub R72 reinforce the binding. To determine the contribution of Site 3 to polyUb binding, we individually mutated residues forming Site 3. With the exception of L415 and L419, mutation of L408, T411, Q418, Q421, or E422 did not disrupt polyUb binding of the tMIU (Fig 5B, F and G). L415 and L419 also bind to the middle Ub (Site 1), and therefore, the loss of binding observed upon mutating these residues could be a result of simultaneously disrupting Site 1 interaction with the middle Ub.

MINDY-1 tMIU binds to K48-linked polyUb chains with higher affinity than MIU2 on its own (Fig 5E and H). We therefore postulate that MIU1 may mediate additional interactions with the distal Ub, which may compensate for the mutations on MIU2 Site 3 (Fig 5J). To test this hypothesis, we mutated residues on Site 3 in MIU2 and found that in the absence of MIU1, mutating L415, Q418, and L419 abolishes binding to polyUb (Fig 5I). This suggests that the residual binding of L415, Q418, and L419 mutants observed in tMIU was due to MIU1 binding to Ub. In addition to highlighting the contribution of Site 3 of MIU2 to Ub binding, these observations suggest that MIU2 binding to the distal Ub is enhanced by MIU1 through mechanisms yet to be elucidated (Fig 5J).

MIU2 A416 and Y424 bind the middle Ub and proximal Ub, respectively, in an orientation that can only be accommodated by K48-linked diUb, which explains the linkage selectivity of MIU2 (Figs EV4A and EV3B). This mode of binding is analogous to Rap80 tUIM, where the linker connecting the two UIMs of Rap80 stretches and positions the interacting surfaces of the two UIMs in an orientation that only K63-linked diUb can accommodate (Fig EV4B) [18,19]. Altering the distance between the key alanine residues of the two UIMs abrogates Rap80 tUIM binding to K63 chains [19]. To test whether MINDY-1 MIU2 also employs the same mode of binding, we altered the distance between the two binding sites within MIU2 by deleting E423 or introducing Ala residues in-between A416 and Y424 (Fig EV4D). Indeed, altering the distance between these two key residues completely disrupts tMIU binding to polyUb chains (Fig EV4D–F). These results highlight the importance of the spatial arrangement of the two Ub-binding sites within MINDY-1 MIU2 to bind Ub moieties within K48-linked polyUb chains.

Individual UIM motifs in Hrs and AIRAPL have been reported to contain multiple Ub-binding sites [20,42]. Hrs UIM has two hydrophobic strips on either side of its helix, which each binds to the I44 patch of independent Ub molecules [42]. The two Ub molecules bound to Hrs are not linked by any isopeptide bond, and therefore, the double-sided Ub-binding on Hrs UIM does not provide linkage specificity but a higher efficiency in binding to multiple monoubiquitylated cargoes in the endocytic pathway [42]. On the

other hand, the tUIM of AIRAPL recognizes K48-linked triUb where the two Ub-binding sites on UIM2 bind to two moieties of Ub simultaneously, whereas UIM1 binds to the proximal Ub [20]. Even though AIRAPL UIM2 was described as the K48 linkage determinant for the tUIM, in the absence of UIM1, AIRAPL UIM2 failed to bind K48-triUb. In contrast, a single MIU motif in MINDY-1, MIU2, uses distinct mechanisms in which the three Ub-binding sites on the MIU simultaneously bind to all three Ub moieties (Fig 5J).

K48-linked polyUb chains are flexible and adopt different conformations as both open and closed chains have been reported for unbound chains [9]. However, all structures of K48-linked diUb chains in complex with their binding partners are found in open conformations where at least one of the two I44 patches is occupied [20,43–47]. The two K48-diUb chains bound to MINDY-1 MIU2 are also in open conformations and suggest a preference for UBDs to bind to K48 chains in more extended conformations (Fig EV2C). In contrast, K63-linked polyUb chains in complex with their binding partners have been observed in both open and closed chain conformations [48]. It is intriguing that none of the UBDs analyzed to date recognize and bind to the closed conformation of K48 chains.

It is interesting that MINDY-1 tMIU, in addition to sensing polyUb chain linkage type, can also select for chain length (Fig 2). In our recent study, we demonstrated that tMIU is required for MINDY-1 DUB activity in hydrolyzing long K48-linked polyUb chains [22]. In the present study, we observe that MINDY-1 MIU2 binds to K48-polyUb chains in open conformations (Fig 5A). We hypothesize that the tMIU helps MINDY-1 bind to long K48 chains and therefore facilitates the DUB to bind to its substrate (Fig EV4G).

Our study also reveals that despite its sequence similarity with MINDY-1 tMIU, FAM63B/MINDY-2 tMIU is completely non-specific for any particular linkage type (Fig 1C). Interestingly, full-length MINDY-2 selectively hydrolyzes only K48 chains [22]. These observations suggest that the tMIU of MINDY-2 may enable the enzyme to process mixed and branched Ub types. Future work will elucidate how the UBD and the catalytic domain of MINDY-1 and MINDY-2 work together in a cellular context.

## Materials and Methods

### cDNA clones and antibodies

All cDNA clones were generated by the DNA cloning team, Medical Research Council Protein Phosphorylation and Ubiquitylation Unit (MRC PPU) Reagents and Services, University of Dundee, United Kingdom (Appendix Table S2). Anti-Ub was purchased from DAKO (Z0458).

### Halo-UBD expression and purification

UBDs were cloned as fusion proteins with an N-terminal GST tag or a tandem GST-Halo tag (Appendix Table S2). Recombinant proteins were expressed in *E. coli* strain BL21 grown in 2× TY media containing 100 μg/ml ampicillin. Cells were induced with 300 μM isopropyl β-D-1-thiogalactopyranoside (IPTG) at an $OD_{600}$ of 0.6–0.8 and grown for 16 h at 16°C. Cells were pelleted and resuspended in 50 mM Tris pH 7.5, 300 mM NaCl, 10% glycerol, 0.075% 2-mercaptoethanol, 1 mM benzamidine, 1 mM AEBSF, and protease inhibitor cocktail (Roche). Cell lysis was carried out by sonication. After being clarified through centrifugation, bacterial lysate was incubated with Glutathione Sepharose 4B resin (GE Healthcare) for 2 h at 4°C. The resin bound proteins were washed extensively with high salt buffer (25 mM Tris pH 7.5, 500 mM NaCl, and 1 mM DTT) and low salt buffer (25 mM Tris pH 7.5, 150 mM NaCl, 10% glycerol, and 1 mM DTT). Halo-tagged UBD was eluted by cleaving off the GST tag using C3 protease. The purified proteins were concentrated, flash frozen in liquid nitrogen and stored at −80°C.

### Assembly and purification of polyubiquitin chains of defined lengths

PolyUb chains were assembled enzymatically in reactions containing 1,500 μM Ub (Sigma Aldrich), 50 mM Tris pH 7.5, 10 mM $MgCl_2$, 0.6 mM DTT, and 10 mM ATP, incubated at 30°C for the indicated period of time. M1 chains were assembled for 2 h in the presence of 1 μM UBE1, 10 μM UBE2L3, and 10 μM HOIP [24]. K6 chains were assembled for 3 h in the presence of 0.5 μM UBE1, 9.5 μM UBE2L3, 12.40 μM NleL (170–782), and 5 μM OTUB1 [25]. K11 chains were assembled for 6 h in the presence of 1 μM UBE1, 40 μM UBE2S-UBP, and 2 μM AMSH [26]. Fresh DUB was added, and the reaction was incubated for another 16 h. K29 chains were assembled for 6 h in the presence of 0.64 μM UBE1, 9.5 μM UBE2D3, and 3 μM UBE3C [27]. K33 chains were assembled for 6 h in the presence of 0.5 μM UBE1, 9 μM UBE2D1, and 6.3 μM AREL1 [28]. In the K29 and K33 chains assembly, DUBs (2 μM vOTU for K29, and 5 μM OTUB1 + 20 μM Cezanne E287K/E288K for K33) were added after the 6-h incubation and the reaction was incubated for another 16 h. K48 chains were assembled for 6 h in the presence of 1 μM UBE1 and 25 μM UBE2R1 [49]. K63 chains were assembled for 3 h in the presence of 1 μM UBE1, 10 μM UBE2N, and 20 μM UBE2V1 [49].

At the end of the assembly reaction, enzymes used in the reaction were precipitated by the addition of a total volume of 50 ml of 50 mM sodium acetate pH 4.5. After at least 3-h incubation at 4°C, the solution was filtered (0.22-μm). DiUb, triUb, tetraUb, and pentaUb were purified by cation exchange using a Resource S 6 ml column (GE Healthcare), equilibrated in 50 mM sodium acetate pH 4.5, and eluted in a gradient with elution buffer (50 mM sodium acetate pH 4.5 and 1 M NaCl). Peak fractions containing di-, tri-, tetra-, and pentaUb chains were concentrated and buffer exchanged to 20 mM Tris pH 7.5.

### UBD linkage selectivity profiling assays

Halo-tagged UBDs (10.5 nmol) were incubated with 100 μl of the HaloLink resin (Promega) in 500 μl of the coupling buffer (50 mM Tris pH 7.5, 150 mM NaCl, 0.05% NP-40 substitute, and 1 mM DTT) for 2 h at 4°C. The UBD linkage selectivity analysis was carried out by incubating 10 μl of the coupled Halo-UBD with 29 pmol of tetraUb of the indicated linkages in 500 μl of pull-down buffer (50 mM Tris pH 7.5, 150 mM NaCl, 0.1% NP-40, 1 mM DTT, 0.5 mg/ml BSA) for 2 h at 4°C. The resin was washed two times with the wash buffer (50 mM Tris pH 7.5, 250 mM NaCl, 0.2% NP-40, 1 mM DTT) and once with the coupling buffer. Captured tetraUb chains were eluted by adding LDS buffer, separated on 4–12%

 

Bis-Tris gel (Thermo Fischer), and visualized by silver staining using Pierce Silver stain kit (ThermoFischer).

#### Isothermal titration calorimetry (ITC)

ITC measurements were performed on a MicroCal PEAQ-ITC (Malvern) at 25°C with a setting of 20 × 2 μl injections. All proteins were dialyzed into 50 mM Hepes pH 7.5, 150 mM NaCl, and 250 μM TCEP. For all measurements, the syringe contained UBD at a concentration of 300 μM, and the cell contained polyUb chains at a concentration of 30 μM.

#### Crystallization and structure determination of MINDY-1 tMIU:K48-diUb

Purified MINDY-1 tMIU and K48-linked diUb were mixed in 1:1 ratio at 400 nmol each. After an 16-h incubation, the protein complex was concentrated to 16.3 mg/ml. Crystals were grown using vapor diffusion technique in mother liquor containing 100 mM sodium acetate pH 5.4 and 18.5% PEG3350. Crystals were cryo-protected in mother liquor containing 30% PEG400 before vitrification in liquid nitrogen. Diffraction data were collected at ID30A of the European Synchrotron Radiation Facility (Grenoble, France). Data were processed and scaled using XDS [50] and merged using AIMLESS [51]. The structure was solved by molecular replacement using Ub (1UBQ [52]) as a search model in Phaser [53]. Iterative rounds of refinements were done using REFMAC5 [54] with model building in COOT [55]. The structure was finally re-refined using PDB_REDO [56]. The final data collection and refinement statistics are shown in Appendix Table S1.

The structure was analyzed with PIC and PISA [57,58]. Figures were made with the PyMOL Molecular Graphics System, Schrödinger, LLC (https://www.pymol.org/).

#### Accession code

Coordinates for MINDY-1 tMIU:K48-diUb complex have been deposited at the Protein Data Bank under accession codes 5MN9.

**Expanded View** for this article is available online.


### Acknowledgements
We thank V.K. Chaugule and S. Lange for discussions and critical comments on the manuscript. This work was supported by the Medical Research Council, UK (MC_UU_12016/6, Ubiquitin signaling mechanisms), Tenovus Scotland, EMBO Young Investigator Programme, and the pharmaceutical companies supporting the Division of Signal Transduction Therapy (AstraZeneca, Boehringer-Ingelheim, GlaxoSmithKline, Merck KGaA, Janssen Pharmaceutica, and Pfizer).


### Author contributions
YAK performed all experiments. YAK and YK designed experiments and analyzed data. SAAR performed crystallographic analyses. SW cloned all the DNA constructs. AK provided enzymes used in the polyUb assembly and K48-polyUb chains used in the ITC experiments. YAK and YK wrote the manuscript with input from all authors.

### Conflict of interest
The authors declare that they have no conflict of interest.

## References


1. Chen ZJ (2005) Ubiquitin signalling in the NF-κB pathway. *Nat Cell Biol* 7: 758 – 765
2. Ulrich HD, Walden H (2010) Ubiquitin signalling in DNA replication and repair. *Nat Rev Mol Cell Biol* 11: 479 – 489
3. MacGurn JA, Hsu P-C, Emr SD (2012) Ubiquitin and membrane protein turnover: from cradle to grave. *Annu Rev Biochem* 81: 231 – 259
4. Bhattacharyya S, Yu H, Mim C, Matouschek A (2014) Regulated protein turnover: snapshots of the proteasome in action. *Nat Rev Mol Cell Biol* 15: 122 – 133
5. Pickart CM, Eddins MJ (2004) Ubiquitin: structures, functions, mechanisms. *Biochim Biophys Acta* 1695: 55 – 72
6. Kulathu Y, Komander D (2012) Atypical ubiquitylation – the unexplored world of polyubiquitin beyond Lys48 and Lys63 linkages. *Nat Rev Mol Cell Biol* 13: 508 – 523
7. Cook WJ, Jeffrey LC, Carson M, Chen Z, Pickart CM (1992) Structure of a diubiquitin conjugate and a model for interaction with ubiquitin conjugating enzyme (E2). *J Biol Chem* 267: 16467 – 16471
8. Cook WJ, Jeffrey LC, Kasperek E, Pickart CM (1994) Structure of tetraubiquitin shows how multiubiquitin chains can be formed. *J Mol Biol* 236: 601 – 609
9. Varadan R, Walker O, Pickart C, Fushman D (2002) Structural properties of polyubiquitin chains in solution. *J Mol Biol* 324: 637 – 647
10. Husnjak K, Dikic I (2012) Ubiquitin-binding proteins: decoders of ubiquitin-mediated cellular functions. *Annu Rev Biochem* 81: 291 – 322
11. Clague MJ, Barsukov I, Coulson JM, Liu H, Rigden DJ, Urbé S (2013) Deubiquitylases from genes to organism. *Physiol Rev* 93: 1289 – 1315
12. He F, Wollscheid H-P, Nowicka U, Biancospino M, Valentini E, Ehlinger A, Acconcia F, Magistrati E, Polo S, Walters KJ (2016) Myosin VI contains a compact structural motif that binds to ubiquitin chains. *Cell Rep* 14: 2683 – 2694
13. Young P, Deveraux Q, Beal RE, Pickart CM, Rechsteiner M (1998) Characterization of two polyubiquitin binding sites in the 26 S protease subunit 5a. *J Biol Chem* 273: 5461 – 5467
14. Hofmann K, Falquet L (2001) A ubiquitin-interacting motif conserved in components of the proteasomal and lysosomal protein degradation systems. *Trends Biochem Sci* 26: 347 – 350
15. Lee S, Tsai YC, Mattera R, Smith WJ, Kostelansky MS, Weissman AM, Bonifacino JS, Hurley JH (2006) Structural basis for ubiquitin recognition and autoubiquitination by Rabex-5. *Nat Struct Mol Biol* 13: 264 – 271
16. Penengo L, Mapelli M, Murachelli AG, Confalonieri S, Magri L, Musacchio A, Di Fiore PP, Polo S, Schneider TR (2006) Crystal structure of the ubiquitin binding domains of Rabex-5 reveals two modes of interaction with ubiquitin. *Cell* 124: 1183 – 1195
17. Hurley JH, Lee S, Prag G (2006) Ubiquitin-binding domains. *Biochem J* 399: 361 – 372
18. Sims JJ, Cohen RE (2009) Linkage-specific avidity defines the lysine 63-linked polyubiquitin-binding preference of Rap80. *Mol Cell* 33: 775 – 783
19. Sato Y, Yoshikawa A, Mimura H, Yamashita M, Yamagata A, Fukai S (2009) Structural basis for specific recognition of Lys 63-linked polyubiquitin chains by tandem UIMs of RAP80. *EMBO J* 28: 2461 – 2468
20. Rahighi S, Braunstein I, Ternette N, Kessler B, Kawasaki M, Kato R, Matsui T, Weiss TM, Stanhill A, Wakatsuki S (2016) Selective binding of AIRAPL tandem UIMs to Lys48-linked tri-ubiquitin chains. *Structure* 24: 412 – 422
21. Burnett B, Li F, Pittman RN (2003) The polyglutamine neurodegenerative protein ataxin-3 binds polyubiquitylated proteins and has ubiquitin protease activity. *Hum Mol Genet* 12: 3195 – 3205

22. Abdul Rehman SA, Kristariyanto YA, Choi SY, Nkosi PJ, Weidlich S, Labib K, Hofmann K, Kulathu Y (2016) MINDY-1 is a member of an evolutionarily conserved and structurally distinct new family of deubiquitinating enzymes. *Mol Cell* 63: 146 – 155
23. Wang Q, Young P, Walters KJ (2005) Structure of S5a bound to monoubiquitin provides a model for polyubiquitin recognition. *J Mol Biol* 348: 727 – 739
24. Stieglitz B, Morris Davies AC, Koliopoulos MG, Christodoulou E, Rittinger K (2012) LUBAC synthesizes linear ubiquitin chains via a thioester intermediate. *EMBO Rep* 13: 840 – 846
25. Hospenthal MK, Freund SMV, Komander D (2013) Assembly, analysis and architecture of atypical ubiquitin chains. *Nat Struct Mol Biol* 20: 555 – 565
26. Bremm A, Freund SMV, Komander D (2010) Lys11-linked ubiquitin chains adopt compact conformations and are preferentially hydrolyzed by the deubiquitinase Cezanne. *Nat Struct Mol Biol* 17: 939 – 947
27. Kristariyanto YA, Abdul Rehman SA, Campbell DG, Morrice NA, Johnson C, Toth R, Kulathu Y (2015) K29-selective ubiquitin binding domain reveals structural basis of specificity and heterotypic nature of K29 polyubiquitin. *Mol Cell* 58: 83 – 94
28. Kristariyanto YA, Choi SY, Abdul Rehman SA, Ritorto MS, Campbell DG, Morrice NA, Toth R, Kulathu Y (2015) Assembly and structure of Lys33-linked polyubiquitin reveals distinct conformations. *Biochem J* 467: 345 – 352
29. Michel MA, Elliott PR, Swatek KN, Simicek M, Pruneda JN, Wagstaff JL, Freund SMV, Komander D (2015) Assembly and specific recognition of K29- and K33-linked polyubiquitin. *Mol Cell* 58: 95 – 109
30. Raasi S, Pickart CM (2005) Ubiquitin chain synthesis. *Methods Mol Biol* 301: 47 – 55
31. Dong KC, Helgason E, Yu C, Phu L, Arnott DP, Bosanac I, Compaan DM, Huang OW, Fedorova AV, Kirkpatrick DS *et al* (2011) Preparation of distinct ubiquitin chain reagents of high purity and yield. *Structure* 19: 1053 – 1063
32. Baboshina OV, Haas AL (1996) Novel multiubiquitin chain linkages catalyzed by the conjugating enzymes E2EPF and RAD6 are recognized by 26 S proteasome subunit 5. *J Biol Chem* 271: 2823 – 2831
33. Sokratous K, Roach LV, Channing D, Strachan J, Long J, Searle MS, Layfield R, Oldham NJ (2012) Probing affinity and ubiquitin linkage selectivity of ubiquitin-binding domains using mass spectrometry. *J Am Chem Soc* 134: 6416 – 6424
34. Shin D, Lee SY, Han S, Ren S, Kim S, Aikawa Y, Lee S (2012) Differential polyubiquitin recognition by tandem ubiquitin binding domains of Rabex-5. *Biochem Biophys Res Commun* 423: 757 – 762
35. Swanson KA, Kang RS, Stamenova SD, Hicke L, Radhakrishnan I (2003) Solution structure of Vps27 UIM-ubiquitin complex important for endosomal sorting and receptor downregulation. *EMBO J* 22: 4597 – 4606
36. Raasi S, Orlov I, Fleming KG, Pickart CM (2004) Binding of polyubiquitin chains to ubiquitin-associated (UBA) domains of HHR23A. *J Mol Biol* 341: 1367 – 1379
37. Chai Y, Berke SS, Cohen RE, Paulson HL (2004) Poly-ubiquitin binding by the polyglutamine disease protein ataxin-3 links its normal function to protein surveillance pathways. *J Biol Chem* 279: 3605 – 3611
38. Pinato S, Scandiuzzi C, Arnaudo N, Citterio E, Gaudino G, Penengo L (2009) RNF168, a new RING finger, MIU-containing protein that modifies chromatin by ubiquitination of histones H2A and H2AX. *BMC Mol Biol* 10: 55
39. Phillips CL, Thrower J, Pickart CM, Hill CP (2001) Structure of a new crystal form of tetraubiquitin. *Acta Crystallogr D Biol Crystallogr* 57: 341 – 344
40. Eddins MJ, Varadan R, Fushman D, Pickart CM, Wolberger C (2007) Crystal structure and solution NMR studies of Lys48-linked tetraubiquitin at neutral pH. *J Mol Biol* 367: 204 – 211
41. Satoh T, Sakata E, Yamamoto S, Yamaguchi Y, Sumiyoshi A, Wakatsuki S, Kato K (2010) Crystal structure of cyclic Lys48-linked tetraubiquitin. *Biochem Biophys Res Commun* 400: 329 – 333
42. Hirano S, Kawasaki M, Ura H, Kato R, Raiborg C, Stenmark H, Wakatsuki S (2006) Double-sided ubiquitin binding of Hrs-UIM in endosomal protein sorting. *Nat Struct Mol Biol* 13: 272 – 277
43. Varadan R, Assfalg M, Raasi S, Pickart C, Fushman D (2005) Structural determinants for selective recognition of a Lys48-linked polyubiquitin chain by a UBA domain. *Mol Cell* 18: 687 – 698
44. Zhang N, Wang Q, Ehlinger A, Randles L, Lary JW, Kang Y, Haririnia A, Storaska AJ, Cole JL, Fushman D *et al* (2009) Structure of the S5a:K48-linked diubiquitin complex and its interactions with Rpn13. *Mol Cell* 35: 280 – 290
45. Liu S, Chen Y, Li J, Huang T, Tarasov S, King A, Weissman AM, Byrd RA, Das R (2012) Promiscuous interactions of gp78 E3 ligase CUE domain with polyubiquitin chains. *Structure* 20: 2138 – 2150
46. Shi Y, Chen X, Elsasser S, Stocks BB, Tian G, Lee B-H, Shi Y, Zhang N, de Poot SAH, Tuebing F *et al* (2016) Rpn1 provides adjacent receptor sites for substrate binding and deubiquitination by the proteasome. *Science* 351: 831
47. Békés M, van der Heden van Noort GJ, Ekkebus R, Ovaa H, Huang TT, Lima CD (2016) Recognition of Lys48-linked di-ubiquitin and deubiquitinating activities of the SARS Coronavirus Papain-like protease. *Mol Cell* 62: 572 – 585
48. Liu Z, Gong Z, Jiang W-X, Yang J, Zhu W-K, Guo D-C, Zhang W-P, Liu M-L, Tang C (2015) Lys63-linked ubiquitin chain adopts multiple conformational states for specific target recognition. *eLife* 4: e05767
49. Komander D, Lord CJ, Scheel H, Swift S, Hofmann K, Ashworth A, Barford D (2008) The structure of the CYLD USP domain explains its specificity for Lys63-linked polyubiquitin and reveals a B box module. *Mol Cell* 29: 451 – 464
50. Kabsch W (2010) XDS. *Acta Crystallogr D Biol Crystallogr* 66: 125 – 132
51. Evans PR, Murshudov GN (2013) How good are my data and what is the resolution? *Acta Crystallogr D Biol Crystallogr* 69: 1204 – 1214
52. Vijay-Kumar S, Bugg CE, Cook WJ (1987) Structure of ubiquitin refined at 1.8 Å resolution. *J Mol Biol* 194: 531 – 544
53. McCoy AJ, Grosse-Kunstleve RW, Storoni LC, Read RJ (2005) Likelihood-enhanced fast translation functions. *Acta Crystallogr D Biol Crystallogr* 61: 458 – 464
54. Vagin AA, Steiner RA, Lebedev AA, Potterton L, McNicholas S, Long F, Murshudov GN (2004) REFMAC5 dictionary: organization of prior chemical knowledge and guidelines for its use. *Acta Crystallogr D Biol Crystallogr* 60: 2184 – 2195
55. Emsley P, Lohkamp B, Scott WG, Cowtan K (2010) Features and development of Coot. *Acta Crystallogr D Biol Crystallogr* 66: 486 – 501
56. Joosten RP, Long F, Murshudov GN, Perrakis A (2014) The PDB_REDO server for macromolecular structure model optimization. *IUCrJ* 1: 213 – 220
57. Tina KG, Bhadra R, Srinivasan N (2007) PIC: protein interactions calculator. *Nucleic Acids Res* 35: W473 – W476
58. Krissinel E, Henrick K (2007) Inference of macromolecular assemblies from crystalline state. *J Mol Biol* 372: 774 – 797
59. Waterhouse AM, Procter JB, Martin DMA, Clamp M, Barton GJ (2009) Jalview version 2–a multiple sequence alignment editor and analysis workbench. *Bioinformatics* 25: 1189 – 1191


 